

Supernova neutrinos and antineutrinos: ternary luminosity diagram and spectral split patterns

Gianluigi Fogli^{1,2}, Eligio Lisi², Antonio Marrone^{1,2} and Irene Tamborra^{1,2}

¹ Dipartimento Interateneo di Fisica “Michelangelo Merlin,”

Via Amendola 173, 70126 Bari, Italy

² Istituto Nazionale di Fisica Nucleare, Sezione di Bari,

Via Orabona 4, 70126 Bari, Italy

Abstract. In core-collapse supernovae, the ν_e and $\bar{\nu}_e$ species may experience collective flavor swaps to non-electron species ν_x , within energy intervals limited by relatively sharp boundaries (“splits”). These phenomena appear to depend sensitively upon the initial energy spectra and luminosities. We investigate the effect of generic variations of the fractional luminosities $(l_e, l_{\bar{e}}, l_x)$ with respect to the usual “energy equipartition” case $(1/6, 1/6, 1/6)$, within an early-time supernova scenario with fixed thermal spectra and total luminosity. We represent the constraint $l_e + l_{\bar{e}} + 4l_x = 1$ in a ternary diagram, which is explored via numerical experiments (in single-angle approximation) over an evenly-spaced grid of points. In inverted hierarchy, single splits arise in most cases, but an abrupt transition to double splits is observed for a few points surrounding the equipartition one. In normal hierarchy, collective effects turn out to be unobservable at all grid points but one, where single splits occur. Admissible deviations from equipartition may thus induce dramatic changes in the shape of supernova (anti)neutrino spectra. The observed patterns are interpreted in terms of initial flavor polarization vectors (defining boundaries for the single/double split transitions), lepton number conservation, and minimization of potential energy.

PACS numbers: 14.60.Pq, 13.15.+g, 97.60.Bw

1. Introduction

Supernova neutrinos and antineutrinos (SN ν and $\bar{\nu}$) have long been studied as probes of both stellar and particle properties [1, 2]. In particular, core-collapse supernovae represent a unique laboratory for studying high-density (anti)neutrino-(anti)neutrino interactions and their associated flavor evolution [3]. Recent results from large-scale calculations [4, 5] have sparked a renewed interest on this topic, which is now the focus of a growing literature, as reviewed in [6, 7]. An interesting outcome of all these studies has been the finding of neutrino flavor changes with similar (“collective”) features over extended energy ranges.

In most supernova scenarios, the flavor evolution can often be reduced to an effective two-family framework (ν_e, ν_x) governed by mass-mixing parameters ($\pm\Delta m^2, \theta_{13}$) [6, 7]. In usual notation, ν_x denotes either ν_μ or ν_τ , or a linear combination of ν_μ and ν_τ (and similarly for antineutrinos). The upper and lower sign of Δm^2 refer to normal and inverted hierarchy, respectively. In these scenarios, collective effects are triggered by any nonzero value of the neutrino mixing angle θ_{13} in inverted hierarchy (in strict analogy with the fall of a inverted pendulum [8]) and end up with a complete exchange (“swap”) of flavor $\nu_e \leftrightarrow \nu_x$ [9, 10] above a “split” energy E_c dictated by $\nu_e - \bar{\nu}_e$ number conservation.

In such effective 2ν scenarios, the paradigm of a single spectral split in the neutrino sector—supported by detailed constructions in adiabatic approximation [11]—has been challenged by the observation of another, low-energy split in the antineutrino sector [12, 13, 14]. Indeed, the joint occurrence of single ν and $\bar{\nu}$ single splits has been recently recognized as a rather general feature in inverted hierarchy, and as a novel possibility in normal hierarchy [15]. Moreover, cases with double ν and $\bar{\nu}$ splits have been identified as well [15]. Relaxing the assumption of energy equipartition has been instrumental in obtaining such multiple split cases.

In general, the total energy luminosity L_{tot} is distributed over six ($3\nu + 3\bar{\nu}$) species,

$$L_{\text{tot}} = L_e + L_{\bar{e}} + 4L_x, \quad (1)$$

or, equivalently,

$$1 = l_e + l_{\bar{e}} + 4l_x, \quad (2)$$

where we have introduced the fractional luminosities

$$l_\alpha = L_\alpha/L_{\text{tot}} \quad (\alpha = e, \bar{e}, x), \quad (3)$$

with $l_x \equiv l_{\bar{x}}$ (we shall often ignore any distinction between ν_x and $\bar{\nu}_x$). The usual assumption of “energy equipartition” amounts to take $l_e = l_{\bar{e}} = l_x$, namely,

$$\text{equipartition} \Leftrightarrow (l_e, l_{\bar{e}}, 4l_x) = (1/6, 1/6, 4/6). \quad (4)$$

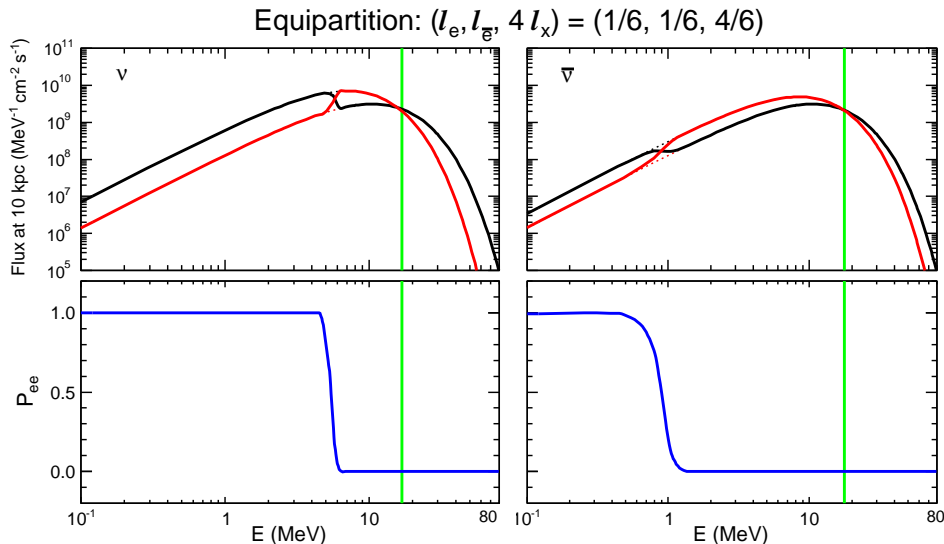


Figure 1. Equipartition case in inverted hierarchy. Left upper panel: flux spectra of ν_e (black, solid) and of ν_x (red, solid) at the end of collective effects; dotted lines indicate initial spectra. All spectra are formally projected at a distance $d = 10$ kpc. Left lower panel: electron flavor survival probability P_{ee} . Right upper and lower panel: as before, but for antineutrinos. Vertical green lines mark the crossing energies where the ν_e (or $\bar{\nu}_e$) and ν_x fluxes are equal.

Figure 1 shows typical results at the end of collective effects (for inverted hierarchy), in a SN scenario endowed with the equipartition hypothesis, as also adopted in our previous papers [12, 13, 14]. The ν_e and ν_x differential fluxes are swapped above a split energy $E_c \simeq 6$ MeV. A similar swap occurs between $\bar{\nu}_e$ and $\bar{\nu}_x$, but at a lower (and not as sharply defined) split energy $\bar{E}_c \sim 1$ MeV. No swap occurs in normal hierarchy for either ν or $\bar{\nu}$ (not shown). Details of the SN scenario will be given in Sec. 3; here we just emphasize that significant (qualitative and quantitative) departures from such results can be induced by admissible deviations from equipartition, such as those considered in [15]. Therefore, it is worthwhile to investigate the spectral dependence upon the initial SN luminosities.

In this work, we perform an extensive phenomenological investigation in a reference SN scenario where all parameters are fixed, except for the fractional luminosities l_α . As described in Sec. 2, the constraint $l_e + l_{\bar{e}} + 4l_x = 1$ [Eq. (2)] is embedded in a “ternary luminosity diagram,” sampled through an evenly-spaced grid of points. Details of the SN model used are given in Sec. 3. Numerical results for inverted hierarchy are described at length in Sec. 4. In particular, abrupt transitions are observed from single to double split cases, across some regions of the ternary diagram surrounding the equipartition case. An interpretation of the results in terms of initial polarization vectors is offered in Sec. 5. Results for normal hierarchy are discussed in Sec. 6. Comments on “more adiabatic” scenarios are provided in Sec. 7. All our findings are briefly summarized in Sec. 8, together with prospects for further work.

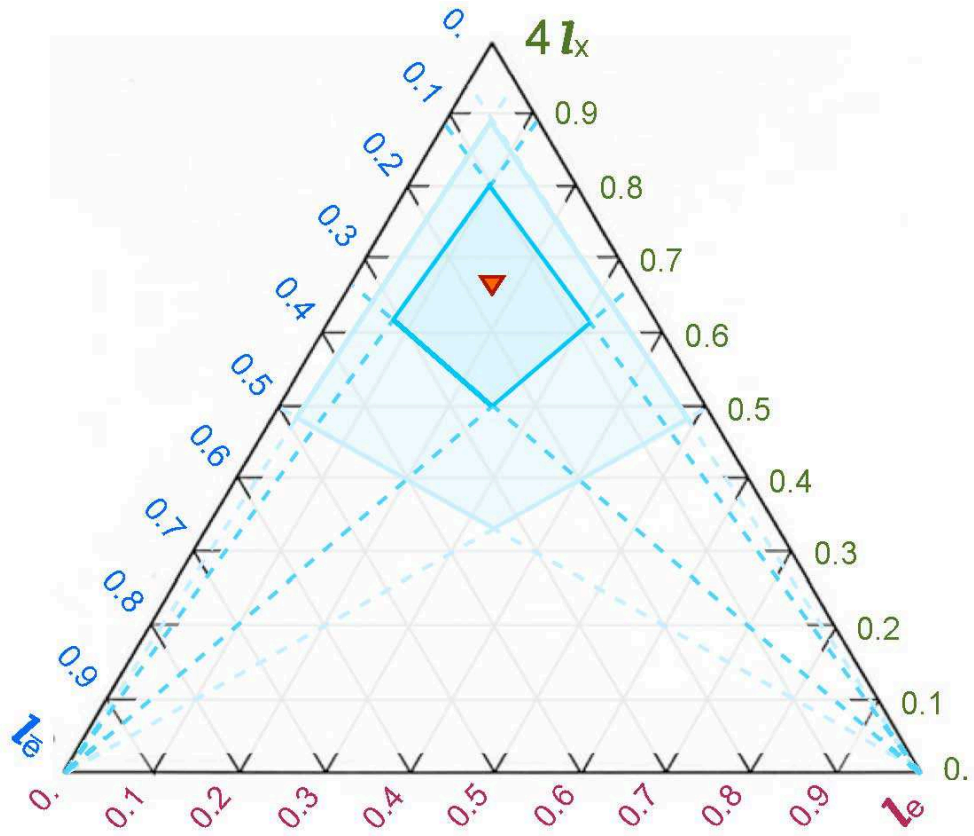


Figure 2. Ternary luminosity diagram. Each point corresponds to fractional luminosities $(l_e, l_{\bar{e}}, 4l_x)$ subject to the constraint $l_e + l_{\bar{e}} + 4l_x = 1$. The equipartition point is marked by a red triangle. The diagram is charted by an evenly-spaced grid of points. The small (large) shaded diamond correspond to ratios l_e/l_x and $l_{\bar{e}}/l_x$ differing from 1 by less than a factor of two (four).

2. Ternary Luminosity Diagram

Unitarity constraints of the form $h_1 + h_2 + h_3 = 1$ can be conveniently represented in ternary diagrams by means of Viviani's theorem [16], where the h_i 's represent the heights projected by any point inside an equilateral triangle of total unit height. In our case [Eq. (2)], the heights are identified with the fractional neutrino energy luminosities: $(h_1, h_2, h_3) = (l_e, l_{\bar{e}}, 4l_x)$.

Figure 2 shows the resulting ternary luminosity diagram. An evenly-spaced grid of points (at intervals $\delta l_e = \delta l_{\bar{e}} = \delta 4l_x = 0.1$) is superposed to guide the eye. A red triangle marks the equipartition point $(l_e, l_{\bar{e}}, 4l_x) = (1/6, 1/6, 4/6)$. Departures from equipartition have often been considered [17]. For instance, Ref. [18] suggests to adopt factor-of-two-uncertainties of the kind $1/2 < l_e/l_x < 2$ and $1/2 < l_{\bar{e}}/l_x < 2$; the corresponding ‘‘allowed region’’ is shown as a shaded inner diamond in Fig. 2. In the same figure, the outer (light-shaded) diamond corresponds to a more conservative allowed region, embracing factor-of-four uncertainties in both l_e/l_x and $l_{\bar{e}}/l_x$.

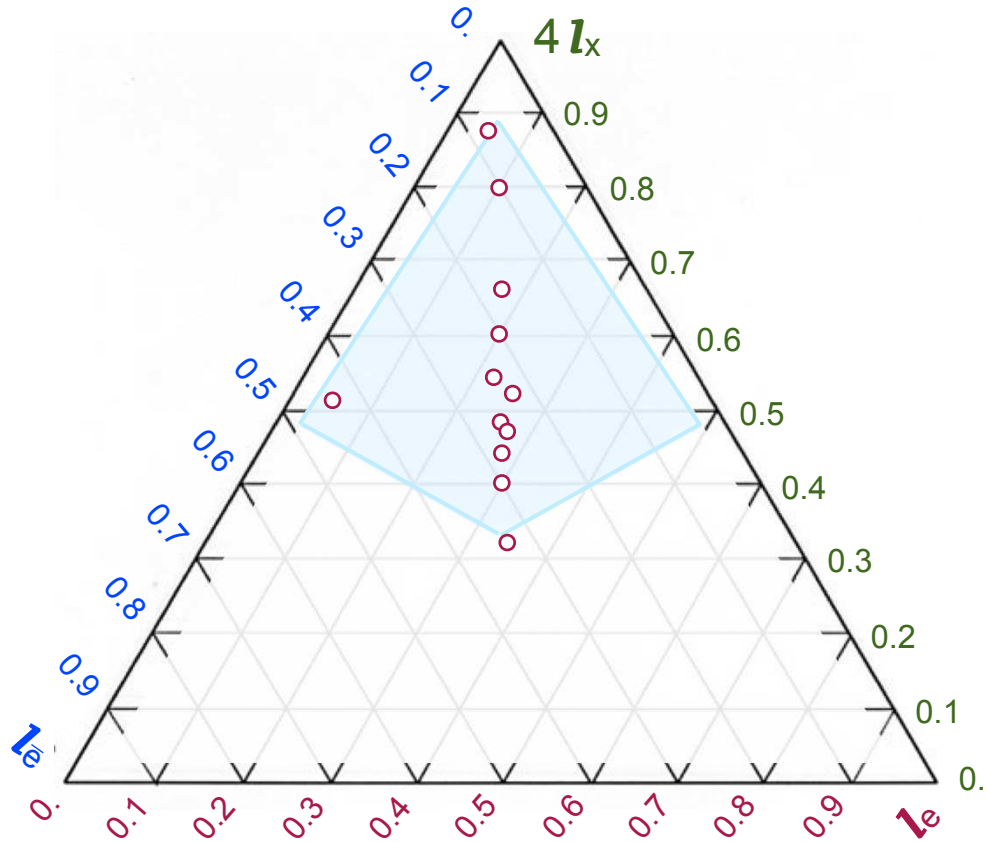


Figure 3. Ternary luminosity diagram. Distribution of luminosities for a set of supernova models, as taken from the compilation in Table 7.3 of Ref. [19].

Figure 3 shows the distribution of fractional luminosities for a set of various supernova simulation outputs, as taken from the compilation reported in Table 7.3 of Ref. [19]. Most of the models cluster around the vertical line $l_{\bar{e}} \sim l_e$, except for one model with very high ratio $l_{\bar{e}}/l_e$ [20]. The overall spread in l_x is rather large. It should be noted that the above models refer to different post-bounce times and different assumptions about SN (astro)physics; see [19] for a critical discussion and comparison. In any case, all such models are basically included in the shaded diamond which corresponds to a factor-of-four uncertainty in l_e/l_x and $l_{\bar{e}}/l_x$, and which will be referred to as the “phenomenologically interesting region.”

In this work we shall mainly focus on such restricted region for the detailed discussion of collective effects; however, for the sake of completeness, we have actually explored the full ternary diagram over all the inner points of the triangular grid, for a total of 36 cases (plus the equipartition one) in either hierarchies. The (computationally demanding) numerical investigation of all such different cases entails some assumptions and approximations, as described in the next Section.

3. Supernova Neutrino Framework

Observations and models of SN explosions suggest a diversity of both initial and time-dependent features, and thus a relatively broad range of possible inputs for SN neutrino studies. We focus on specific SN inputs in terms of luminosities, spectra, geometry, frequencies, evolution equations, and selected approximations, as described below.

3.1. Neutrino luminosities and spectra

In previous works [12, 13, 14], inspired by the SN model in [21], we have assumed a total SN binding energy $E_B \simeq 3 \times 10^{53}$ erg, and a typical luminosity decay timescale $\tau \simeq 3$ s. At early times ($t \ll \tau$), where large deviations from the equipartition hypothesis may take place [17, 22], these choices suggests a total luminosity

$$L_{\text{tot}} \simeq 10^{53} \text{ erg/s} , \quad (5)$$

which we fix as input, while leaving free the fractional luminosities $l_\alpha = L_\alpha/L_{\text{tot}}$.

Concerning average energies, we adopt typical early-time values [17, 22],

$$\langle E_e \rangle = 10 \text{ MeV}, \quad \langle E_{\bar{e}} \rangle = 12 \text{ MeV}, \quad \langle E_x \rangle = 15 \text{ MeV}. \quad (6)$$

Finally, the initial (normalized) energy spectra $\Phi_\alpha(E)$ are assumed to be thermal,

$$\Phi_\alpha(E) = \frac{2\beta_\alpha}{3\zeta_3} \frac{(\beta_\alpha E)^2}{e^{(\beta_\alpha E)} + 1} , \quad (7)$$

where $\zeta_3 \simeq 1.202$ and β_α is an inverse temperature parameter ($\beta = 1/T$) [12], equal to

$$\beta_\alpha = \frac{c_+}{\langle E_\alpha \rangle} = \begin{cases} 0.315 \text{ MeV}^{-1} & (\alpha = e) , \\ 0.263 \text{ MeV}^{-1} & (\alpha = \bar{e}) , \\ 0.210 \text{ MeV}^{-1} & (\alpha = x) , \end{cases} \quad (8)$$

with

$$c_+ = \frac{7\pi^4}{180\zeta_3} \simeq 3.151 . \quad (9)$$

3.2. Geometry

We assume a bulb model [5] with neutrinosphere radius

$$R_\nu = 10 \text{ km} . \quad (10)$$

We also adopt the so-called single-angle approximation, where neutrino-neutrino interactions are averaged along a single, radial trajectory [5]. In this case, for $r > R_\nu$, the effective ν_α number density per unit of volume and energy is given by [5]

$$n_\alpha(r, E) = \frac{L_{\text{tot}} l_\alpha}{4\pi R_\nu^2} \frac{\Phi_\alpha(E)}{\langle E_\alpha \rangle} g(r) , \quad (11)$$

where $g(r)$ is a geometrical damping factor,

$$g(r) = \left[1 - \sqrt{1 - \left(\frac{R_\nu}{r} \right)^2} \right]^2 , \quad (12)$$

decreasing from unity to zero as $\sim 1/r^4$. (See however [23] for a somewhat different function $g(r)$ proposed in the single-angle limit.) Integration over energy provides the effective ν_α density per unit volume,

$$N_\alpha(r) = \int dE n_\alpha(r, E) = c(r) l_\alpha \beta_\alpha , \quad (13)$$

where

$$c(r) = \frac{L_{\text{tot}}}{4\pi R_\nu^2} \frac{g(r)}{c_+} . \quad (14)$$

For definiteness, the absolute fluxes per unit of energy,

$$F_\alpha(E) = \frac{L_{\text{tot}} l_\alpha}{4\pi d^2} \frac{\Phi_\alpha(E)}{\langle E_\alpha \rangle} , \quad (15)$$

will always be projected at a typical galactic-center distance of

$$d = 10 \text{ kpc} , \quad (16)$$

for both initial and intermediate spectra (at the end of collective effects).

3.3. Frequencies

In general, the most relevant frequencies in the context of SN neutrino collective effects are the vacuum oscillation frequency ω , the matter potential profile $\lambda(r)$, and the neutrino potential profile $\mu(r)$. We neglect the subdominant vacuum frequency driven by the smallest (“solar”) δm^2 and the tiny ν_μ - ν_τ matter potential difference which, as discussed in [14], produce only very small effects even at early times in our SN model; see also [24].

The vacuum frequency reads

$$\omega = \frac{\Delta m^2}{2E} = \frac{5.07}{E/\text{MeV}} [\text{km}^{-1}] , \quad (17)$$

where $\Delta m^2 = 2 \times 10^{-3} \text{ eV}^2$ has been taken. We shall consider the energy range $E \in [0.1, 80] \text{ MeV}$, corresponding to $\omega \in [0.06, 50] \text{ km}^{-1}$. Note that, as nicely shown in [15], the collective ν and $\bar{\nu}$ dynamics merge in the limit $\omega \rightarrow 0$, namely at high E (at least in an effective 2ν description).

The matter potential $\lambda(r) = \sqrt{2} G_F N_e(r)$ (where N_e is the electron number density) can, to a large extent, be rotated away in the equations of motion [4]. However, matter effects play a role, e.g., in delaying the start-up of collective effects [8], modifying some low-energy split features [13], generating later resonance effects for relatively large θ_{13} (see, e.g., [6]), and possibly inducing early decoherence [25]. By neglecting $\lambda(r)$, one trades such possible effects for a significant speed-up of the numerical calculations, which is a relevant gain in our systematic exploration of the ternary diagram. Therefore, in the spirit of Ref. [15], we choose to neglect λ from the beginning, and to focus on the dominant effects generated by the neutrino interaction potential μ .

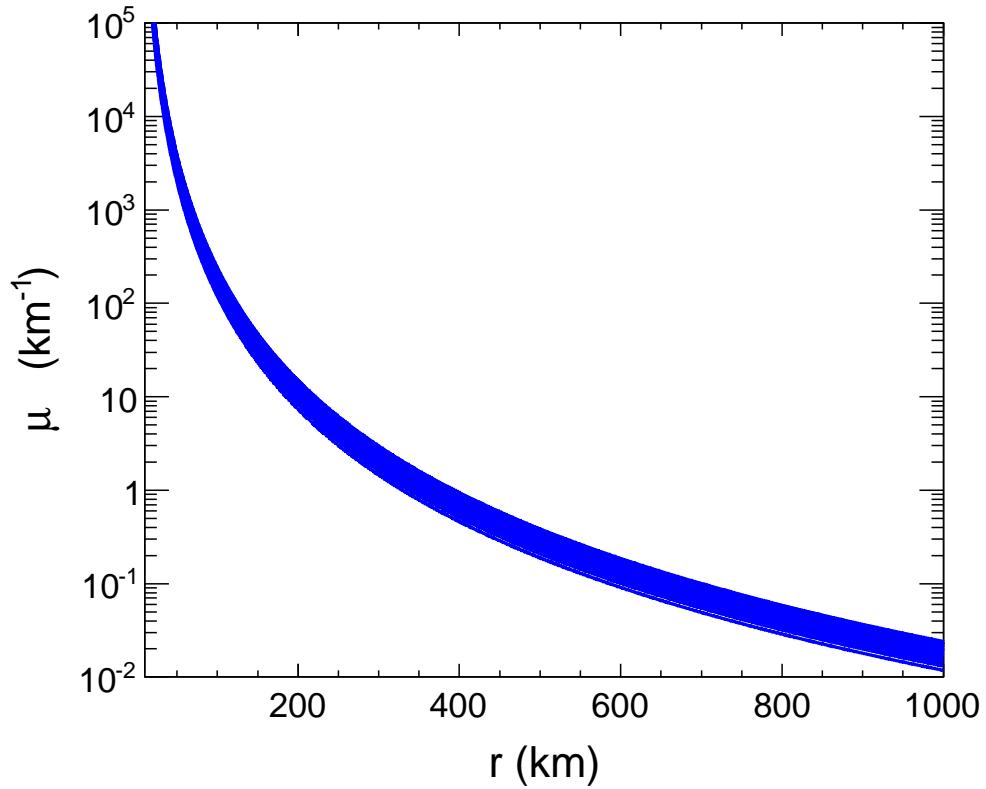


Figure 4. Neutrino interaction potential $\mu(r)$ for our supernova model, in the radial range $r \in [10, 10^3]$ km. The vertical spread is a consequence of slight variations of the curves $\mu(r)$ over different grid points of the ternary luminosity diagram.

The μ radial profile is given by

$$\mu(r) = \sqrt{2}G_F(N + \bar{N}) , \quad (18)$$

where, as we shall argue below, the appropriate ν and $\bar{\nu}$ number densities (N and \bar{N} , respectively) refer to an effective 2ν scenario, namely

$$N = N_e + N_x , \quad \bar{N} = N_{\bar{e}} + N_{\bar{x}} , \quad (19)$$

so that

$$\mu(r) = c(r) (l_e \beta_e + l_{\bar{e}} \beta_{\bar{e}} + 2l_x \beta_x) . \quad (20)$$

Figure 4 shows the corresponding family of $\mu(r)$ curves (too close to be distinguishable) in our adopted SN model, as obtained by varying the fractional luminosities l_α over the 36 grid points in the ternary diagram.

Collective effects are expected to vanish when $\mu(r)$ is somewhat below the smallest vacuum frequency considered, $\omega_{\min} \simeq 0.06 \text{ km}^{-1}$. We have verified that such vanishing is numerically realized within $r < 10^3$ km at any grid point; for safety, calculations are extended to $r = 10^3$ km in all cases.

3.4. Flavor evolution formalism

In the paper [14] we have performed detailed three-flavor calculations for our SN model at the equipartition point for different times. The results of [14] show that, up to small effects at the percent (or lower) level, the collective dynamics basically involve only two neutrino species (ν_e, ν_x), while the $\nu_{\mu,\tau}$ combination orthogonal to ν_x remains a ‘‘spectator’’ neutrino species, and similarly for antineutrinos; see also [26]. For instance, a typical spectral swap can be thought to occur between ν_e and one of the two species ν_x , the other being unaffected during collective evolution. The spectator species enters, however, in the later evolution at large radius via the usual θ_{12} mixing effects [26]. By focusing our attention on the main collective effects within $r < 10^3$ km, we can then reduce the full 3ν evolution to an effective 2ν one, namely: $3\nu = (\nu_e, \nu_x) \oplus \nu_x$, where the relevant 2ν subspace (ν_e, ν_x) is governed by $(\pm\Delta m^2, \theta_{13})$. As in [14], we choose a default value

$$\sin^2 \theta_{13} = 10^{-6} . \quad (21)$$

We have explicitly verified, for several (non-equipartition) test cases in our SN scenario, that the effective 2ν calculations [with $\mu(r)$ defined as in Eq. (20)] reproduce the results obtained from a full 3ν approach [14] within percent accuracy.

Concerning the 2ν framework, we adopt the same notation of [12] in terms of single-mode Bloch vectors \mathbf{P} and $\bar{\mathbf{P}}$ in flavor space, appropriately extended to generic fractional luminosities l_α . In particular, the initial conditions for the global polarization vectors \mathbf{J} , $\bar{\mathbf{J}}$ and for their difference $\mathbf{D} = \mathbf{J} - \bar{\mathbf{J}}$, are given by:

$$\mathbf{J} = \frac{1}{N + \bar{N}} \int dE (n_e - n_x) \mathbf{z} = \frac{l_e \beta_e - l_x \beta_x}{l_e \beta_e + l_{\bar{e}} \beta_{\bar{e}} + 2l_x \beta_x} \mathbf{z} , \quad (22)$$

$$\bar{\mathbf{J}} = \frac{1}{N + \bar{N}} \int dE (n_{\bar{e}} - n_{\bar{x}}) \mathbf{z} = \frac{l_{\bar{e}} \beta_{\bar{e}} - l_x \beta_x}{l_e \beta_e + l_{\bar{e}} \beta_{\bar{e}} + 2l_x \beta_x} \mathbf{z} , \quad (23)$$

$$\mathbf{D} = \frac{1}{N + \bar{N}} \int dE (n_e - n_{\bar{e}}) \mathbf{z} = \frac{l_e \beta_e - l_{\bar{e}} \beta_{\bar{e}}}{l_e \beta_e + l_{\bar{e}} \beta_{\bar{e}} + 2l_x \beta_x} \mathbf{z} . \quad (24)$$

Note that the integrand in \mathbf{J} is positive (negative) for energies below (above) the crossing energy where the ν_e and ν_x fluxes are equal, and similarly for $\bar{\mathbf{J}}$; see also Fig. 1. The D_z component of \mathbf{D} is a constant of motion, corresponding to $\nu_e - \bar{\nu}_e$ number conservation [8].

Finally, we remind that a potential energy \mathcal{V} can be attached to the system,

$$\mathcal{V} \simeq \mp \mathbf{z} \cdot (\mathbf{W} + \bar{\mathbf{W}}) , \quad (25)$$

where the upper (lower) sign refers to normal (inverted) hierarchy. The global vectors \mathbf{W} and $\bar{\mathbf{W}}$ are defined by energy integrals analogous to \mathbf{J} and $\bar{\mathbf{J}}$ in the above equations, but with a further factor ω in the integrand [12]. Therefore, also such vectors receive positive (negative) contributions below (above) the crossing energies. The role of the crossing energies in understanding single and multiple splits has been emphasized in [15].

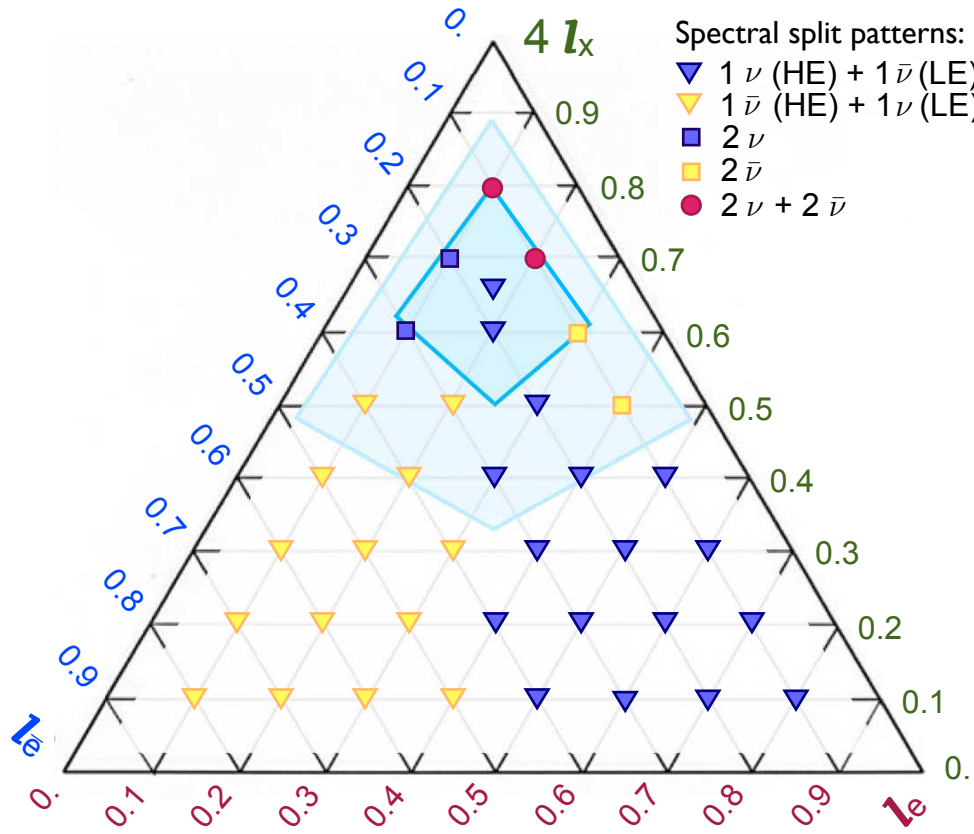


Figure 5. Spectral split patterns in inverted hierarchy. Blue triangles: one “high-energy” ν split and one “low-energy” $\bar{\nu}$ split. Blue squares: two ν splits (and no $\bar{\nu}$ split). Yellow triangles and squares: as before, but with ν and $\bar{\nu}$ interchanged. Red circles: two splits for both ν and $\bar{\nu}$.

4. Results for Inverted Hierarchy: Description

Figure 5 shows the qualitative spectral split patterns emerging from our numerical exploration of the ternary luminosity diagram, in the case of inverted hierarchy. In the lower half of the diagram, corresponding to relatively low ν_x luminosity ($4l_x < 0.5$), we always find one ν and one $\bar{\nu}$ split. More precisely, the blue triangles on the right correspond to one dominant ν split at high energy (HE) plus a minor $\bar{\nu}$ split at low energy (LE), qualitatively similar to Fig. 1; for the yellow triangles on the left, the situation is reversed for ν and $\bar{\nu}$. As the ν_x luminosity increases, some 1ν (HE) + 1ν (LE) split cases survive (blue triangles), including the equipartition point. However, these cases are now flanked, on the left, by a couple of points where a double ν split occurs (blue squares) and, on the right, by two points with a double $\bar{\nu}$ split (yellow squares) plus two points with a double split for both ν and $\bar{\nu}$ (red circles). Therefore, a complex phenomenology of multiple splits [15] emerges in the ternary diagram, even if restricted to the region of phenomenological interest (the largest shaded diamond). In particular, small departures from luminosity equipartition can abruptly change the split patterns.

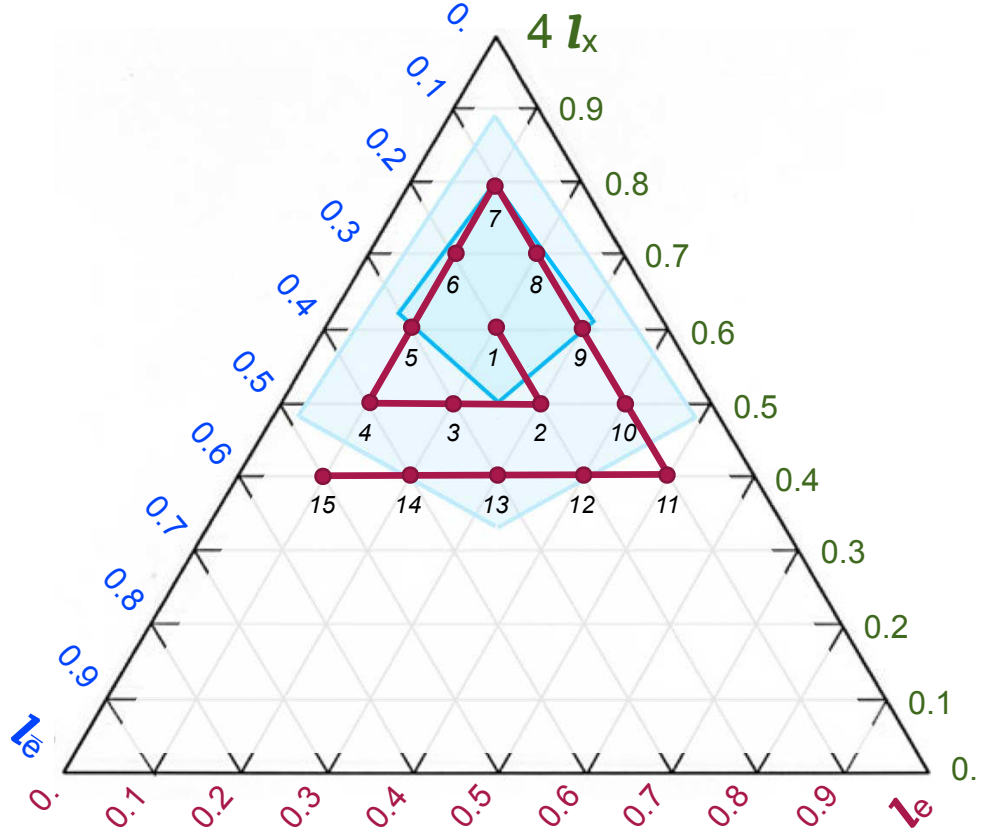


Figure 6. Representative grid points (numbered from 1 to 15), which cover all the observed split patterns. The points define a trajectory which starts close to the equipartition case and then spirals outwards.

In order to better appreciate these changes, quantitative results will be shown for representative grid points. Figure 6 shows fifteen selected points, forming a trajectory which starts close to the equipartition case and then spirals outwards. This trajectory allows to explore the region of phenomenological interest, and to cover all the five (qualitatively different) single and double split patterns described in the comment to Fig. 5. The corresponding spectra are discussed next.

Figures 7, 8 and 9 show the oscillated fluxes of neutrino (left) and antineutrinos (right) per unit energy, at the end of collective effects ($r < 10^3$ km). The black and red solid curves refer to e -flavor and x -flavor, respectively; dotted curves represent unoscillated fluxes. Vertical green lines mark crossing energies, where fluxes of different flavor intersect, and flavor changes—if any—are unobservable. It is worth noticing that, in all cases, the unoscillated fluxes have qualitatively similar features, despite the large differences in relative luminosities: the ν_x flux is always lower (higher) than the ν_e flux, for energies below (above) the crossing energy E_c , which ranges between 10 and 30 MeV; and similarly for antineutrinos, with \bar{E}_c in the range 5–30 MeV. Nevertheless, oscillated fluxes show large differences from point to point. In all panels, we indicate the point number (from 1 to 15) on the left, and the luminosity values (l_e , $l_{\bar{e}}$, $4l_x$) on the right.

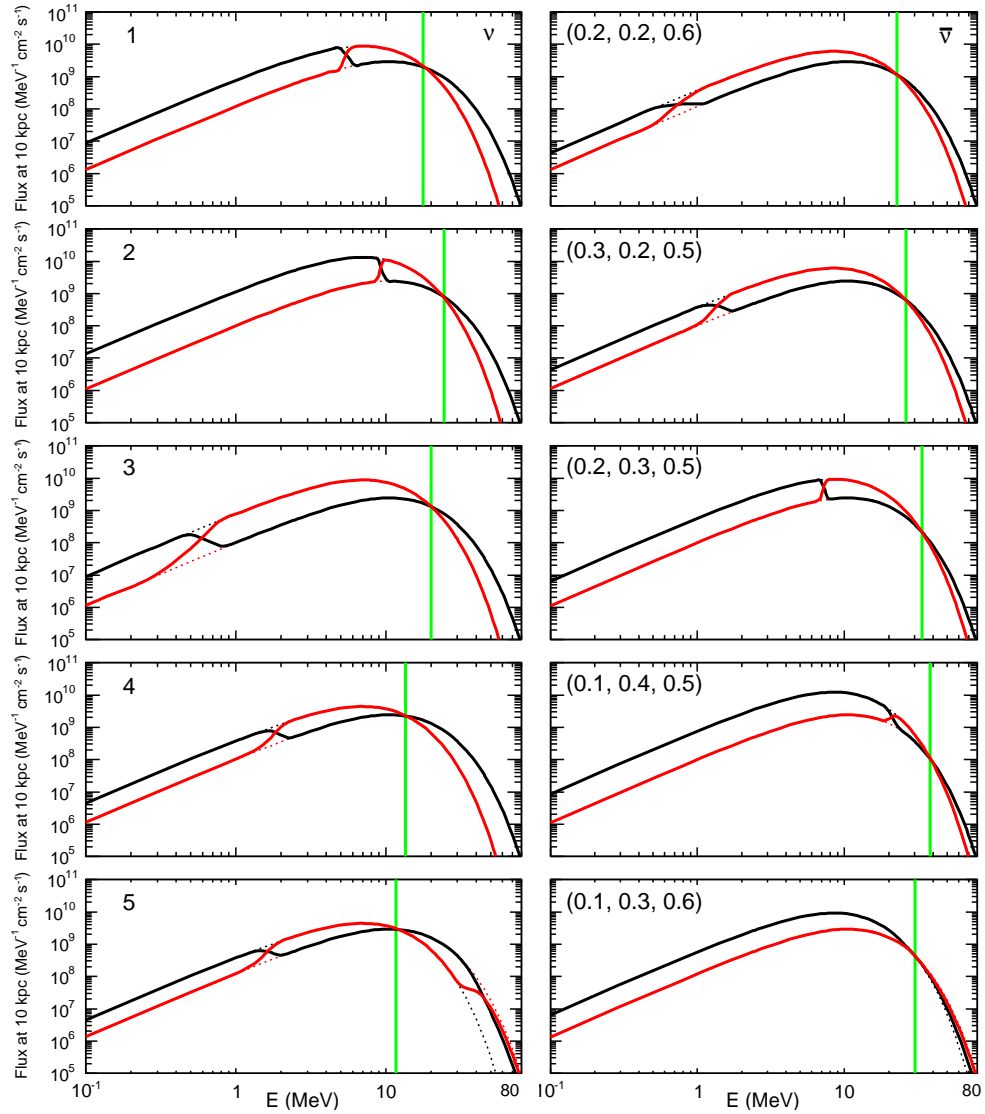


Figure 7. Neutrino (left) and antineutrino (right) energy spectra at the end of collective effect, for the points 1–5 in Fig. 6. The corresponding fractional luminosities (l_e , $l_{\bar{e}}$, l_x) are indicated in each right panel. Vertical green lines mark the crossing energies where the ν_e (or $\bar{\nu}_e$) and ν_x fluxes are equal.

In Fig. 7, both the 1st and the 2nd point show a split pattern very similar to the equipartition case in Fig. 1, with a sharp HE ν split and a broader, LE $\bar{\nu}$ split. The situation is suddenly reversed in the 3rd and 4th point, showing a sharp HE $\bar{\nu}$ split and a broader, LE ν split. The split pattern changes again in the 5th point, where a second split appears for ν 's above the crossing energy, while no evident flavor change emerges for $\bar{\nu}$'s (up to small effects in the upper tail of the spectrum).

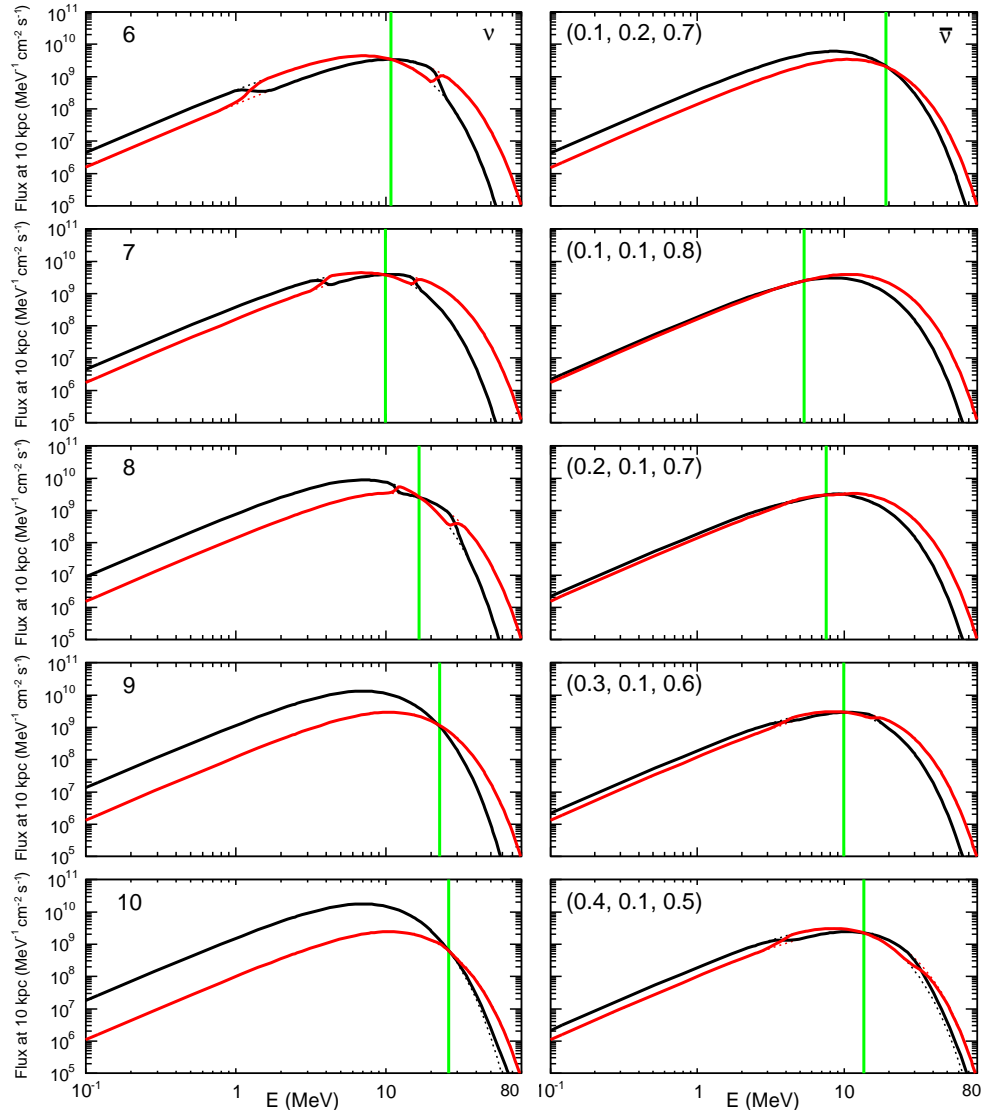


Figure 8. As in Fig. 7, but for points 6–10.

In Fig. 8, the 6th point shows a split pattern similar to the last one in the previous figure, namely, a double ν split and no $\bar{\nu}$ split. However, in both the 7th and 8th point, a double split occurs also for $\bar{\nu}$'s, although the closeness of the $\bar{\nu}_e$ and $\bar{\nu}_x$ spectra make it difficult to appreciate it graphically (it will be shown in a different way below). The 9th and 10th point show a more evident $\bar{\nu}$ double split, but no ν flavor change (up to small upper-tail effects in the last case). The grid points 5–10 exhaust the cases where we find a double split in ν and/or $\bar{\nu}$ spectra.

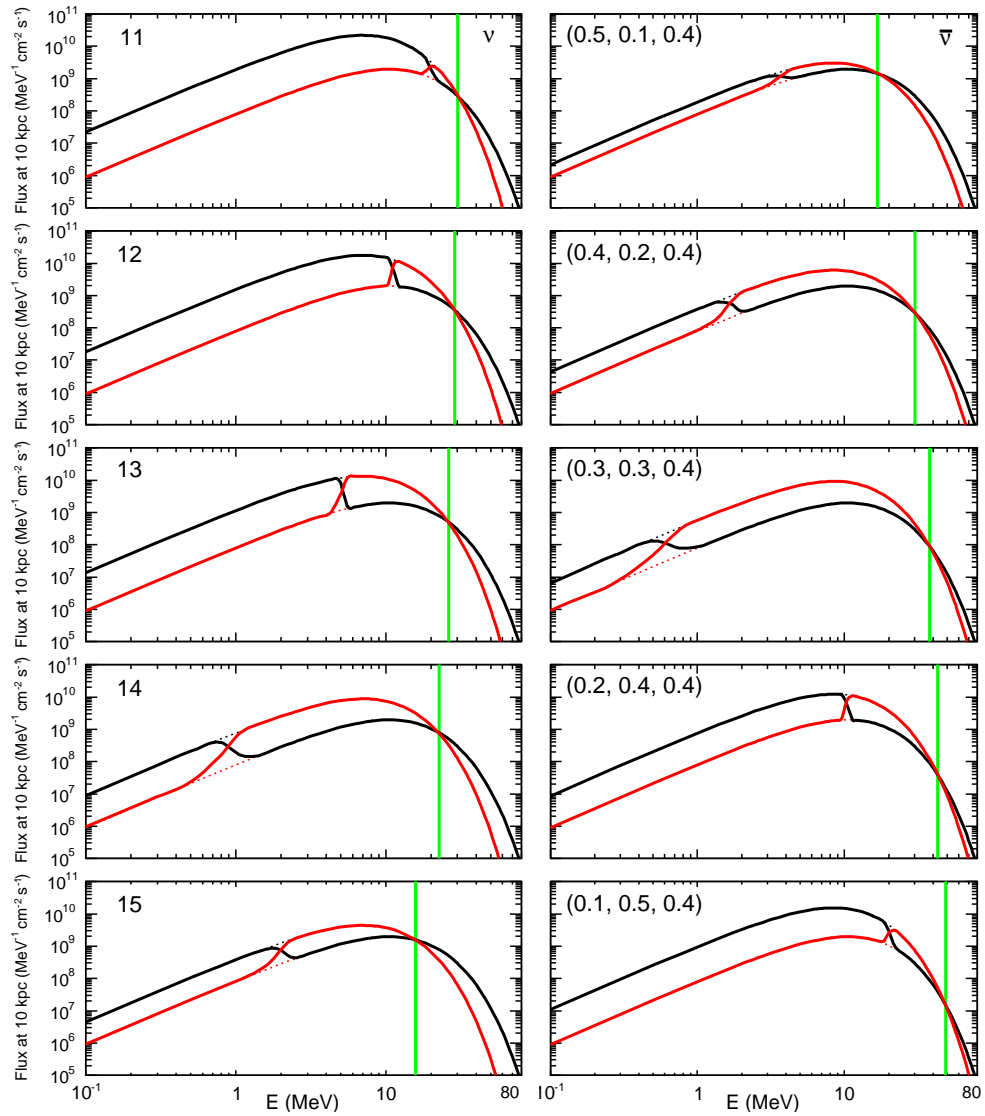


Figure 9. As in Fig. 7, but for points 11–15.

In Fig. 9, the cases from 11 to 13 show a pattern with a sharp HE ν split and a broader LE $\bar{\nu}$ split, while the situation is suddenly reversed in the last two (14th and 15th) cases. It should be noted that the sudden exchange of roles between ν and $\bar{\nu}$ across cases 13 and 14 occurs despite the fact the unoscillated spectra and the crossing energies are very similar.

In general, the results of Figs. 7–9 suggest the existence of a sort of “phase transitions” in the ternary diagram, with abrupt changes in the split patterns when the initial luminosities cross some “phase boundaries,” which we shall try to identify in the next Section.

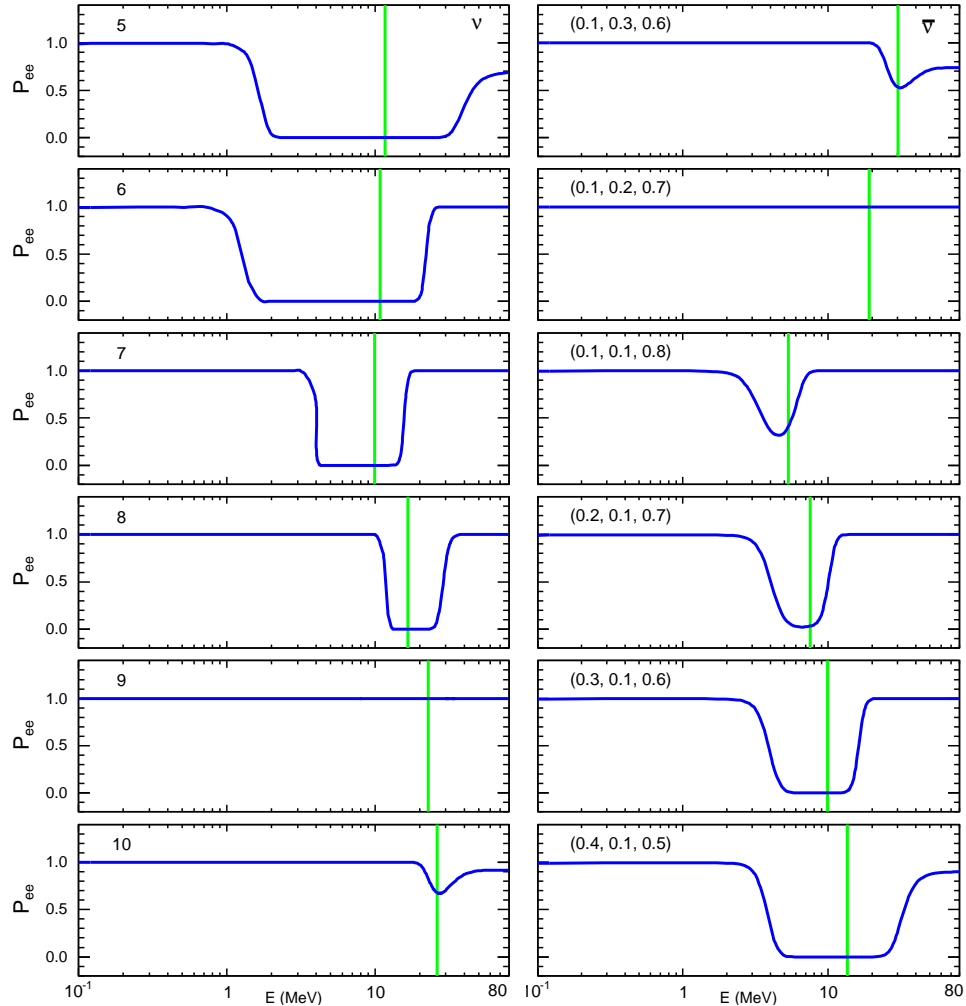


Figure 10. Survival probability P_{ee} for neutrinos (left) and antineutrinos (right) in each of six points 5–10 of Fig. 6, where a double split is observed for neutrinos and/or antineutrinos.

Finally, Fig. 10 shows the e -flavor survival probability profile for neutrinos (left) and antineutrinos (right), for the six grid points numbered from 5 to 10 (see Fig. 6), where double splits occur in either ν or $\bar{\nu}$ or both (see Fig. 5). All double splits flank the crossing energy (vertical green line), in agreement with the arguments of [15]. As also noted in [15], the values of P_{ee} for ν and $\bar{\nu}$ coincide at high E (i.e., for $\omega \rightarrow 0$).

A double-double split is evident only in cases 7 and 8. In cases 5 and 10, instead, there seems to be a partly developed “would-be double split” for $\bar{\nu}$ and ν , respectively. In the spirit of [15], it is tempting to attribute the suppression of such emerging splits to the relatively high (thus unfavorable [15]) values of the associated crossing energies; however, this argument is insufficient to explain the total absence of $\bar{\nu}$ and ν double splits in cases 6 and 9, where the associated crossing energies are favorably lower. In the next Sec. 5, we shall develop different arguments, trying to relate (at least some of) such spectral features to global initial conditions and potential energy minimization. Additional comments will be provided in Sec. 7.

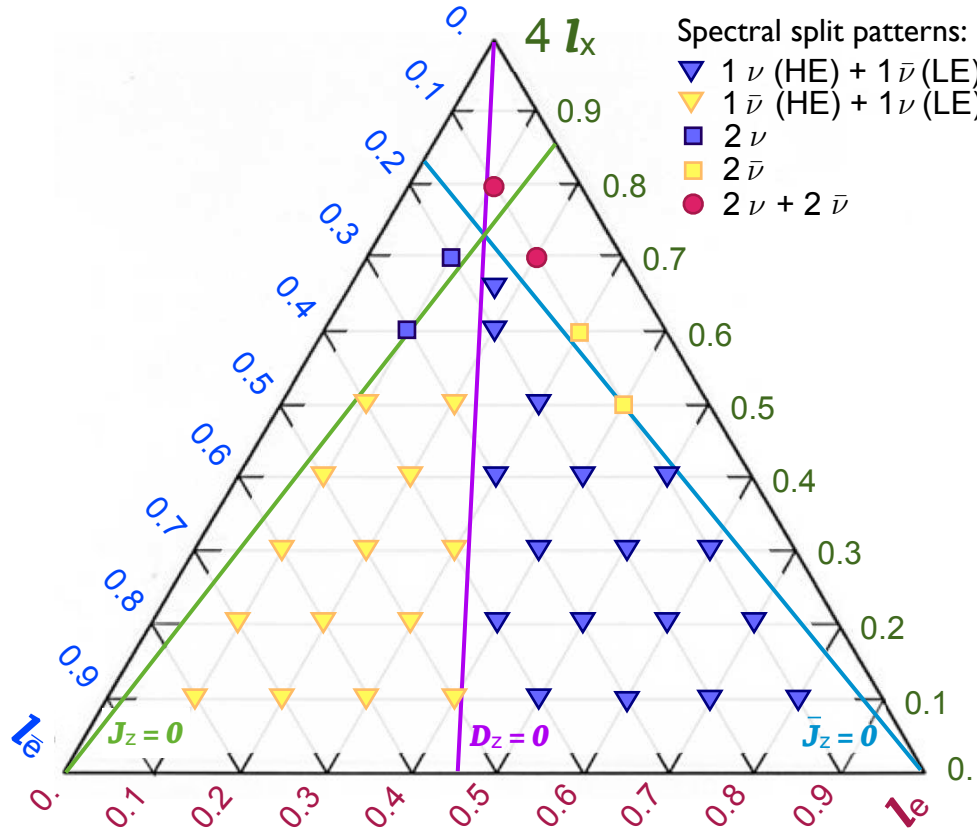


Figure 11. Spectral split patterns, superposed to the three lines characterized by $J_z = 0$ (green, with $J_z > 0$ below the line), by $\bar{J}_z = 0$ (blue, with $\bar{J}_z > 0$ below the line), and where $D_z = 0$ (violet, with $D_z > 0$ on the right of the line). The lines mark transitions to different split patterns.

5. Results for Inverted Hierarchy: Interpretation

The authors of [15] propose a very interesting attempt to explain analytically the development and the stabilization of spectral splits in terms of adiabatic invariants, energy minimization, and localization of the crossing energies (with details to appear in a forthcoming paper). Here we aim at providing another viewpoint on the interpretation of single and double spectral splits, with emphasis on the initial orientation of the global polarization vectors and on some non-adiabatic features.

Initially, the global polarization vectors \mathbf{J} , $\bar{\mathbf{J}}$ and \mathbf{D} are oriented along the \mathbf{z} axis. Figure 11 displays the curves (straight lines in our SN model) where $J_z = 0$ (green), $\bar{J}_z = 0$ (blue) and $D_z = 0$ (violet) at the neutrinosphere, superposed to the same marked grid of points of Fig. 5. We surmise that sign changes of J_z , \bar{J}_z and D_z across these lines mark “phase transitions” across different split patterns in the ternary diagram, as argued below for the various cases reproduced from Fig. 5 (blue and yellow triangles and squares, red circles).

5.1. Cases with $1\nu(HE) + 1\bar{\nu}(LE)$ split: blue triangles

These cases, which include the equipartition one, are characterized by $J_z > 0$, $\bar{J}_z > 0$, and $D_z > 0$. In other words, both \mathbf{J} and the smaller vector $\bar{\mathbf{J}}$ are initially aligned upwards, in the unstable pendulum position [8]. As already argued in [12], the flavor pendulum dynamics would bring both vectors downwards, but is impeded by conservation of D_z ; the simplest way to minimize the potential energy is then to invert the vector $\bar{\mathbf{J}}$ and an equivalent fraction of the vector \mathbf{J} , leading to a sharply defined “high-energy” neutrino split (whose development can be described by detailed adiabatic constructions [11]).

However, the “low-energy” antineutrino split seem to have a different, nonadiabatic origin, as already argued in [13] and suggested by its broader features. In the present work (where the effects of the matter potential λ are ignored), we find that the $\bar{\nu}$ modes below the split energy \bar{E}_s basically experience a usual “resonant transition” when $-\omega + \mu D_z \simeq 0$, and then decouple from the collective dynamics. In the energy range considered ($E \geq 0.1$ MeV), this resonance is highly nonadiabatic, and leads to a two-level hopping probability $P_C \simeq 1$, corresponding to $P_{ee} \simeq 1$. [We have explicitly verified the expected decrease of P_C and P_{ee} at lower energies, as well as their dependence on the $d \log \mu / dr$ profile.] In other words, the low-energy neutrino modes resonate with the interaction potential, and do not participate in later collective swaps. We find that this phenomenon roughly takes place during (and a little bit after) the so-called period of synchronized oscillations [27] (which is then followed by “bipolar” oscillations [28]). Defining μ_s as the value of μ at the transition from synchronized to bipolar oscillations [12], the antineutrino energy modes which remain pinned upwards are roughly determined by the condition $\omega > \mu_s D_z$. In our numerical experiments, such condition identifies the antineutrino split energies within a factor of about 2–3; in particular, we find that the highest values of such energies are reached for the grid points closest to the $D_z = 0$ line.

5.2. Cases with $1\nu(LE) + 1\bar{\nu}(HE)$ split: yellow triangles

These cases are similar to the previous one, but the roles of ν and $\bar{\nu}$ are exchanged, since $D_z < 0$ and thus \bar{J}_z is larger than J_z . The dominant HE split, dictated by D_z -conservation, occurs for antineutrinos. The inversion of low-energy neutrino modes appears to be impeded by early nonadiabatic resonances for $\omega > -\mu_s D_z$.

5.3. Cases with 2ν splits: blue squares

In these two cases (identified as n. 5 and 6 in Figs. 6 and 10), \mathbf{J} is oriented upwards, in the unstable position, while $\bar{\mathbf{J}}$ is oriented downwards and is thus already stable. However, the vector \mathbf{J} cannot be inverted, even partially (i.e., with a single split), due to D_z conservation: the two vectors are “locked” and remain basically equal in modulus and orientation at the end of collective effects, as we have explicitly verified. However,

one can still invert a fraction of the neutrino spectra “symmetrically” with respect to E_c [15], so as to preserve the modulus of \mathbf{J} while decreasing the value of W_z (and thus the potential energy). The double neutrino split appears thus a highly constrained way to lower the energy of the system, when the global polarization vectors of ν and $\bar{\nu}$ are basically locked.

Finally, we note that the point identified as n. 5 in Figs. 6 and 10 represents a “borderline” case, being almost on top of the line at $J_z = 0$. This specific feature might be at the origin of the partial “double split,” barely emerging in the antineutrino spectrum for this case (see Fig. 10).

5.4. Cases with $2\bar{\nu}$ splits: yellow squares

These two cases (numbered as points n. 9 and 10 in Figs. 6 and 10) are analogous to the previous ones (n. 6 and 5, respectively), but the role of ν and $\bar{\nu}$ is exchanged. So, the same considerations apply, including the “borderline” features of point 10 which sits on top of the $\bar{J}_z = 0$ line.

A third case (numbered as point n. 8 in Figs. 6 and 10) should also fall in the same category, being characterized by the same initial signs of the global polarization vectors. However, for this point (the lowest red circle in Fig. 11) we find double splits for both ν and $\bar{\nu}$ (see Fig. 10). We have been unable to explain this “exception” by sharpening energy minimization arguments. See, however, Sec. 7 for further comments.

5.5. Cases with $2\nu + 2\bar{\nu}$ splits: red circles

These cases include the mentioned point n. 8 (which escapes a simple explanation) and point n. 7 (the highest red circle in Fig. 11), which can be instead more easily interpreted. The latter point is the only one, in our grid, having both \mathbf{J} and $\bar{\mathbf{J}}$ initially oriented downward, in the stable pendulum position. Then, the only way to further minimize the potential energy (without altering D_z) is to generate double splits which preserve the moduli of \mathbf{J} and $\bar{\mathbf{J}}$ while decreasing the values of W_z and \bar{W}_z , which is indeed what happens at the end of the collective evolution (see Fig. 10).

5.6. Summary for inverted hierarchy

In inverted hierarchy, both single and double splits may appear in either the ν or the $\bar{\nu}$ spectra, depending on the initial distribution of the total luminosity over the species ($\nu_e, \bar{\nu}_e, \nu_x$). The split patterns observed numerically admit (with one exception) a relatively simple interpretation in terms of initial conditions for the global polarization vectors $\mathbf{J}, \bar{\mathbf{J}}$ and \mathbf{D} , supplemented by arguments related to the flavor pendulum dynamics and its potential energy minimization. Transitions to different split patterns emerge when crossing the lines $J_z = 0, \bar{J}_z = 0$ and $D_z = 0$ in the ternary luminosity diagram.

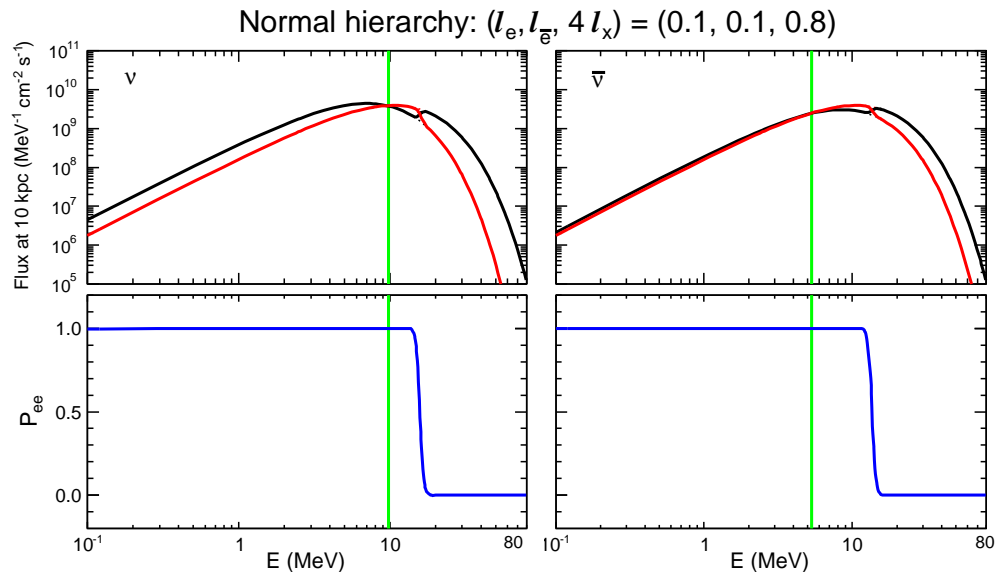


Figure 12. Normal hierarchy: spectra for the single grid point where splits are observed. For all other grid points, collective effects do not change the original spectra.

6. Results for Normal Hierarchy

In normal hierarchy, the flavor pendulum dynamics is generally trivial, since the initial conditions are typically very close to the stable equilibrium position [8]. However, an interesting counterexample has been provided in [15] for a situation with relatively large ν_x luminosity.

In our ternary diagram, we find that collective effects produce no flavor change in normal hierarchy, except for a single grid point—the one with the highest ν_x luminosity. In this peculiar case, both \mathbf{J} and $\bar{\mathbf{J}}$ start in the unstable position (now corresponding to downward orientation), and then partially reverse, in order to minimize energy while preserving D_z . As a result, single splits emerge in both ν and $\bar{\nu}$ spectra, as shown in Fig. 12, in qualitative agreement with the normal-hierarchy case discussed in [15].

7. Comments on a “more adiabatic” scenario

In Sec. 5, the proposed interpretation of the double split patterns emerging in Fig. 10 shows that initially stable (downward-aligned) global polarization vectors may be (cases 7, 8) or may not be (cases 5, 6, and 9, 10) further stabilized by a double split. In view of the results in [15], it is worthwhile to investigate if the absence of some “would-be double splits” can be related to incomplete adiabaticity. To this purpose, we examine a hypothetical scenario, where the function $\mu(r)$ is radially stretched by a factor of ten above the neutrinosphere,

$$\mu(r) \rightarrow \mu \left(R_\nu + \frac{r - R_\nu}{10} \right). \quad (26)$$

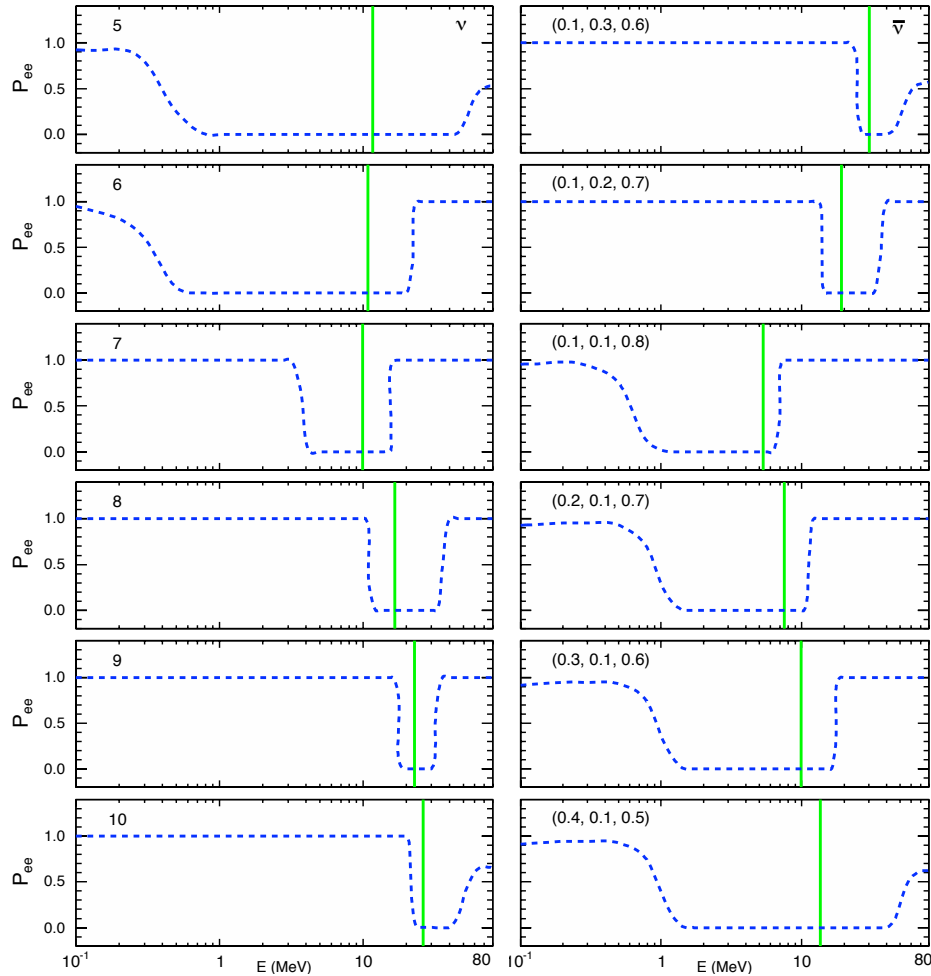


Figure 13. As in Fig. 10, but for the “more adiabatic” $\mu(r)$ profile in Eq. (26).

The main results for such “more adiabatic” scenario are summarized in Fig. 13. A comparison with the analogous Fig. 10 shows that the increased adiabaticity make $2\nu + 2\bar{\nu}$ splits emerge in all cases 5–10. In particular, for cases 5 and 6, we find that the “new” double splits provide a further (although quantitatively small) decrease of the potential energy for $\bar{\nu}$'s, which already start from stable initial conditions ($\bar{J}_z < 0$); and analogously for ν 's in cases 9 and 10. In other words, the ν or $\bar{\nu}$ systems seem to have “enough time” to relax further, and to minimize an already low potential energy. Note also that the split energies are somewhat different in Fig. 13 as compared with Fig. 10, especially on the low-energy side, where we have already argued (Sec. 5.1) that nonadiabatic resonances play a prominent role. In general, more adiabatic profiles for $\mu(r)$ [such as in Eq. (26)] seem to cancel qualitative differences among the different double split cases commented in Secs. 5.3, 5.4 and 5.5, which merge in the single $2\nu + 2\bar{\nu}$ case described in Sec. 5.5. Conversely, all single-split cases remain qualitatively similar, as we have explicitly verified by numerical exploration of the ternary diagram.

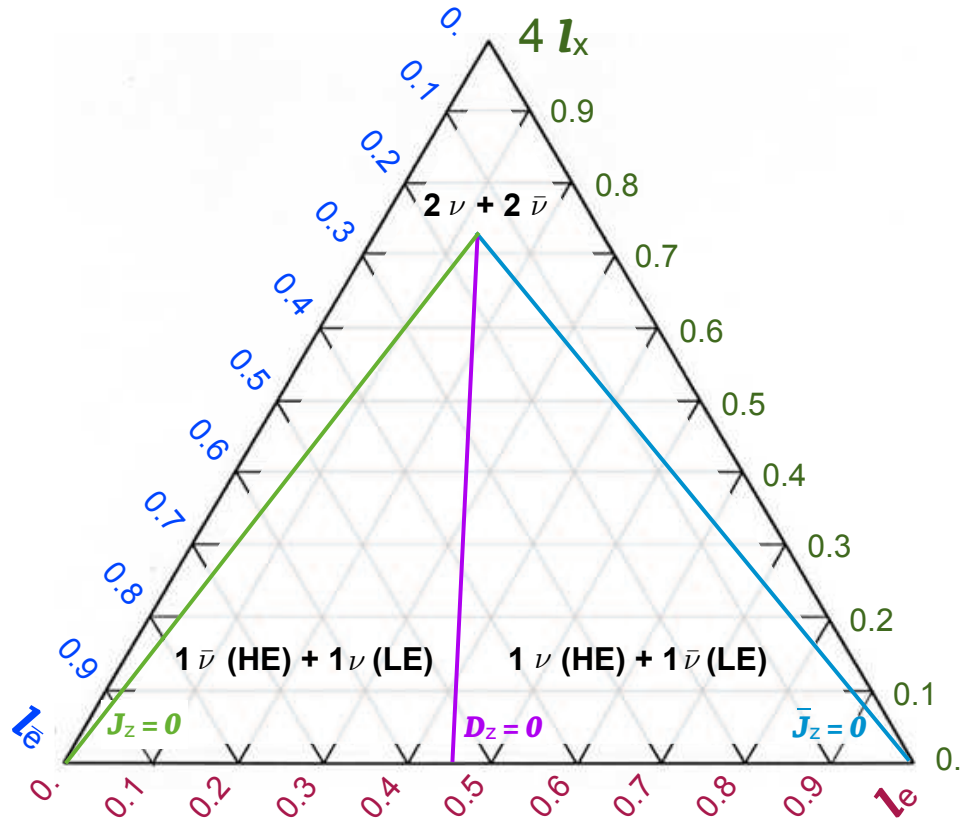


Figure 14. Spectral split patterns for a scenario with increased adiabaticity (see the text for details). The lines, as in Fig. 11, mark transitions to different split patterns.

Figure 14 shows the resulting, “adiabatic” spectral split patterns, to be compared with the ones in Fig. 11. It appears that there are at least three distinct “phases” in the ternary diagram, with either single splits (at low/high or high/low energy) or double splits in the ν and $\bar{\nu}$ spectra. Within the $2\nu + 2\bar{\nu}$ region of Fig. 14, possible sub-phases seem to emerge as a result of incomplete adiabaticity in Fig. 11.

The equipartition case is close to the crossing point of the three curves in Figs. 11 and 14. Therefore, in the inverted hierarchy case, relatively small variations in the fractional luminosities, or in the (non)adiabatic character of the neutrino evolution, may induce significant variations in the observable spectral split patterns.

Concerning the normal hierarchy case, we do not find qualitatively new features by using the modified function $\mu(r)$ in Eq. (26), as compared with the discussion in Sec. 6.

8. Summary and Prospects

In core-collapse supernovae, collective effects involving high-density (anti)neutrinos continues to reveal surprising features. In particular, relatively small variations of the luminosities associated to ν_e , $\bar{\nu}_e$ and ν_x appear to trigger abrupt changes from single- to double-split features in the energy spectra.

We have investigated the effect of generic variations of the fractional luminosities $(l_e, l_{\bar{e}}, 4l_x)$ with respect to the usual “energy equipartition” case $(1/6, 1/6, 4/6)$, within an early-time supernova scenario with fixed thermal spectra and total luminosity. The constraint $l_e + l_{\bar{e}} + 4l_x = 1$ has been embedded in a “ternary luminosity diagram,” which has been numerically explored over an evenly-spaced grid of points.

In inverted hierarchy, we have found both single- and double-split cases for either neutrino or antineutrino spectra, and have proposed an interpretation of these patterns in terms of initial orientations of the global flavor polarization vectors \mathbf{J} and $\bar{\mathbf{J}}$, and of minimization of the potential energy, constrained by lepton number conservation ($D_z = J_z - \bar{J}_z = \text{const}$). In particular, the curves defined by $J_z = 0$, $\bar{J}_z = 0$ and $D_z = 0$ appear to provide “phase transition boundaries” between regions with single- and double-split features. The regions where at least one double split occurs (for either ν or $\bar{\nu}$) can actually merge into a single one with $2\nu + 2\bar{\nu}$ splits, if adiabaticity is increased by design. It turns out that the luminosity equipartition point is relatively close to the crossing point of the three separation curves; therefore, relatively small variations of the fractional luminosities can produce qualitatively different swaps and quantitatively significant changes in the final spectra, at the end of the collective flavor evolution.

On one hand, these results may provide a handle to reconstruct the original luminosities $(l_e, l_{\bar{e}}, 4l_x)$, if the associated spectral split patterns can be observed in future galactic SN explosions. On the other hand, they complicate the calculation of the diffuse supernova neutrino background, since past SN events may well have different relative luminosities and thus different spectral split features. Even within a single core-collapse SN event, there might be transitions from single- to double-split spectra (or viceversa) during the first few seconds after bounce, as a results of time-dependent changes in the relative luminosities, average energies, (non)adiabatic features, and possible departures from thermal spectra.

The analysis of this rich phenomenology is just at the beginning, and calls for a deeper theoretical interpretations and for more refined numerical explorations, in order to get the most from observable supernova neutrino events. Concerning the results presented in this work, we plan to refine them by focusing on the phenomenologically interesting region close to the equipartition point, where further insights on the spectral split patterns may be expected, in both normal and inverted hierarchy, by adopting a more general SN framework and a denser sampling grid.

Acknowledgments

This work is supported in part by the Italian “Istituto Nazionale di Fisica Nucleare” (INFN) and “Ministero dell’Istruzione, dell’Università e della Ricerca” (MIUR) through the “Astroparticle Physics” research project. We also acknowledge support by the E.U. (ENTApP network). I.T. thanks the organizers of the TAUP’09 Conference, where preliminary results of this work were presented, for kind hospitality.

References

- [1] G. Raffelt, *Stars as Laboratories for Fundamental Physics* (U. of Chicago Press, Chicago, 1996), 664 pp.
- [2] H. T. Y. Janka, K. Langanke, A. Marek, G. Martinez-Pinedo and B. Mueller, “Theory of Core-Collapse Supernovae,” *Phys. Rept.* **442**, 38 (2007) [arXiv:astro-ph/0612072].
- [3] J. T. Pantaleone, “Neutrino oscillations at high densities,” *Phys. Lett. B* **287**, 128 (1992).
- [4] H. Duan, G. M. Fuller and Y. Z. Qian, “Collective Neutrino Flavor Transformation In Supernovae,” *Phys. Rev. D* **74**, 123004 (2006) [arXiv:astro-ph/0511275].
- [5] H. Duan, G. M. Fuller, J. Carlson and Y. Z. Qian, “Simulation of coherent non-linear neutrino flavor transformation in the supernova environment. I: Correlated neutrino trajectories,” *Phys. Rev. D* **74**, 105014 (2006) [arXiv:astro-ph/0606616].
- [6] A. Dighe, “Physics potential of future supernova neutrino observations,” *Proceedings of Neutrino 2008*, 23rd International Conference on Neutrino Physics and Astrophysics (Christchurch, New Zealand, 2008) *J. Phys. Conf. Ser.* **136**, 022041 (2008) [arXiv:0809.2977 [hep-ph]].
- [7] H. Duan and J. P. Kneller, “Neutrino flavour transformation in supernovae,” arXiv:0904.0974 [astro-ph.HE].
- [8] S. Hannestad, G. G. Raffelt, G. Sigl and Y. Y. Y. Wong, “Self-induced conversion in dense neutrino gases: Pendulum in flavour space,” *Phys. Rev. D* **74**, 105010 (2006) [Erratum-ibid. *D* **76**, 029901 (2007)] [arXiv:astro-ph/0608695].
- [9] G. G. Raffelt and A. Y. Smirnov, “Self-induced spectral splits in supernova neutrino fluxes,” *Phys. Rev. D* **76**, 081301 (2007) [Erratum-ibid. *D* **77**, 029903 (2008)] [arXiv:0705.1830 [hep-ph]].
- [10] H. Duan, G. M. Fuller, J. Carlson and Y. Q. Zhong, “Neutrino Mass Hierarchy and Stepwise Spectral Swapping of Supernova Neutrino Flavors,” *Phys. Rev. Lett.* **99**, 241802 (2007) [arXiv:0707.0290 [astro-ph]].
- [11] G. G. Raffelt and A. Y. Smirnov, “Adiabaticity and spectral splits in collective neutrino transformations,” *Phys. Rev. D* **76**, 125008 (2007) [arXiv:0709.4641 [hep-ph]].
- [12] G. L. Fogli, E. Lisi, A. Marrone and A. Mirizzi, “Collective neutrino flavor transitions in supernovae and the role of trajectory averaging,” *JCAP* **0712**, 010 (2007) [arXiv:0707.1998 [hep-ph]].
- [13] G. L. Fogli, E. Lisi, A. Marrone, A. Mirizzi and I. Tamborra, “Low-energy spectral features of supernova (anti)neutrinos in inverted hierarchy,” *Phys. Rev. D* **78**, 097301 (2008) [arXiv:0808.0807 [hep-ph]].
- [14] G. Fogli, E. Lisi, A. Marrone and I. Tamborra, “Supernova neutrino three-flavor evolution with dominant collective effects,” *JCAP* **0904**, 030 (2009) [arXiv:0812.3031 [hep-ph]].
- [15] B. Dasgupta, A. Dighe, G. G. Raffelt, and A. Y. Smirnov, “Multiple Spectral Splits of Supernova Neutrinos,” *Phys. Rev. Lett.* **103**, 051105 (2009) [arXiv:0904.3542 [hep-ph]].
- [16] Eric W. Weisstein: “Viviani’s Theorem.” From MathWorld – A Wolfram Web Resource: mathworld.wolfram.com/VivianisTheorem.html
- [17] G. G. Raffelt, M. T. Keil, R. Buras, H. T. Janka and M. Rampp, “Supernova neutrinos: Flavor-dependent fluxes and spectra,” *Proceedings of NOON 2003*, 4th Workshop on Neutrino Oscillations and their Origin (Kanazawa, Japan, 2003), edited by Y. Suzuki, M. Nakahata,

- Y. Itow, M. Shiozawa and Y. Obayashi (World Scientific, Singapore, 2004), p. 380. [arXiv:astro-ph/0303226].
- [18] C. Lunardini and A. Y. Smirnov, "Probing the neutrino mass hierarchy and the 13-mixing with supernovae," JCAP **0306**, 009 (2003) [arXiv:hep-ph/0302033].
- [19] M. T. Keil, PhD dissertation "Supernova neutrino spectra and applications to flavor oscillations" (Technical U., Munich, 2003) arXiv:astro-ph/0308228.
- [20] H.-T. Janka and W. Hillebrandt, "Neutrino emission from type II supernovae—an analysis of the spectra," Astron. Astrophys. **224**, 49 (1989).
- [21] R. C. Schirato and G. M. Fuller "Connection between supernova shocks, flavor transformation, and the neutrino signal," arXiv:astro-ph/0205390.
- [22] T. Totani, K. Sato, H. E. Dalhed and J. R. Wilson, "Future detection of supernova neutrino burst and explosion mechanism," Astrophys. J. **496**, 216 (1998) [arXiv:astro-ph/9710203].
- [23] B. Dasgupta, A. Dighe, A. Mirizzi, and G. G. Raffelt, "Collective neutrino oscillations in non-spherical geometry," Phys. Rev. D **78**, 033014 (2008) [arXiv:0805.3300 [hep-ph]].
- [24] A. Esteban-Pretel, S. Pastor, R. Tomas, G. G. Raffelt and G. Sigl, "Mu-tau neutrino refraction and collective three-flavor transformations in supernovae," Phys. Rev. D **77**, 065024 (2008) [arXiv:0712.1137 [astro-ph]].
- [25] A. Esteban-Pretel, A. Mirizzi, S. Pastor, R. Tomas, G. G. Raffelt, P. D. Serpico and G. Sigl, "Role of dense matter in collective supernova neutrino transformations," Phys. Rev. D **78**, 085012 (2008) [arXiv:0807.0659 [astro-ph]].
- [26] B. Dasgupta and A. Dighe, "Collective three-flavor oscillations of supernova neutrinos," Phys. Rev. D **77**, 113002 (2008) [arXiv:0712.3798 [hep-ph]].
- [27] S. Pastor, G. G. Raffelt and D. V. Semikoz, "Physics of synchronized neutrino oscillations caused by self-interactions," Phys. Rev. D **65**, 053011 (2002) [arXiv:hep-ph/0109035].
- [28] H. Duan, G. M. Fuller, J. Carlson and Y. Z. Qian, "Analysis of Collective Neutrino Flavor Transformation in Supernovae," Phys. Rev. D **75**, 125005 (2007) [arXiv:astro-ph/0703776].